AXIAL COMPRESSIVE BEHAVIOR OF SQUARE AND RECTANGULAR HIGH-STRENGTH CONCRETE-FILLED FRP TUBES

Togay OZBAKKALOGLU*

ABSTRACT

This paper presents results of an experimental study on the behavior of square and rectangular high-strength concrete (HSC)-filled fiber reinforced polymer (FRP) tubes (HSCFFTs) under concentric compression. The effects of the tube thickness, sectional aspect ratio and corner radius on the axial compressive behavior of concrete-filled FRP tubes (CFFTs) were investigated experimentally through the tests of 24 CFFTs that were manufactured using unidirectional carbon fiber sheets and high-strength concrete (HSC) with 78 MPa average compressive strength. As the first experimental investigation on the axial compressive behavior of square and rectangular HSCFFTs, the results of the study reported herein allows a number of significant conclusions to be drawn. First and foremost, test results indicate that sufficiently confined square and rectangular HSCFFTs can exhibit highly ductile behavior. The results also indicate that confinement effectiveness of FRP tubes increases with an increase in corner radius and decreases with an increase in sectional aspect ratio. It is also observed and discussed that HSCFFTs having tubes of low confinement effectiveness may experience a significant strength loss at the point of transition on their stress-strain curves. Furthermore, it is found that the behavior of HSCFFTs at this region differ from that of normal-strength CFFTs and it is more sensitive to the effectiveness of confining tube. Examination of the test results have also lead to a number of important observations on the influence of the key confinement parameters on the development and distribution of the hoop strains on the tubes of CFFTs, which are presented and discussed in the paper.

KEYWORDS: Fiber reinforced polymers (FRP); High-strength concrete (HSC); Columns; Confinement; Tubes; Stress-strain behavior.

* Senior Lecturer, School of Civil, Environmental and Engineering, University of Adelaide, Australia. Tel : + 618 8303 6477; Fax : +618 8303 4359; Email: tozbakka@civeng.adelaide.edu.au

INTRODUCTION

Over the past two decades the use of externally bonded fiber reinforced polymers (FRP) has become widely accepted for strengthening reinforced concrete members. As an important application of FRP composites, confinement of existing reinforced concrete columns with FRP jackets have been investigated extensively (e.g, Rochette and Labossiere 2000; Xiao and Wu 2000; Pessiki et al. 2001; Chaallal et al. 2003; De Lorenzis and Tepfers 2003; Lam and Teng 2004; Hadi 2006; Ilki et al. 2008; Wang and Wu 2008; Eid et al. 2009; Ozcan et al. 2010; Dai et al. 2011). More recently, attention has turned to the potential applications of FRP composites for new structures. One such application, which has received much recent attention (e.g. Mirmiran et al. 1998; Seible et al. 1999; Fam and Rizkalla 2001, 2002; Fam et al. 2005; Shao and Mirmiran 2005; Ozbakkaloglu and Saatcioglu 2006, 2007; Zaghi et al. 2012), involves the use of concrete-filled FRP tubes (CFFTs) as high-performance composite columns in earthquake-resistant construction of new structures. Existing studies have demonstrated the ability of CFFTs to develop very high inelastic deformation capacities under simulated seismic loading, which makes them an attractive alternative for construction of new earthquake-resistant columns (Yamakawa et al. 2003; Shao and Mirmiran 2005; Ozbakkaloglu and Saatcioglu 2006, 2007; Saatcioglu et al. 2008).

It is well understood that lateral confinement can enhance both the strength and ductility of concrete. CFFTs owe their improved deformation capacities to the confinement action provided by the surrounding FRP tube. Therefore, to develop a rational procedure for designing CFFTs as earthquake-resistant columns in new construction, it is necessary to understand and be able to model the effects of FRP confinement on the stress-strain behavior of concrete in CFFTs. This requires a comprehensive investigation on the axial compressive behavior of CFFTs. A number of such studies have been reported in the literature. However, the majority of these studies have been concerned with circular CFFTs (Mastrapa 1997; Saafi et al. 1999; Tegola and Manni 1999;

Mirmiran et al. 2001; Moss 2001; Mandal et al. 2005; Zhu et al. 2005; Li 2006; Mohamed and Masmoudi 2010; Park et al. 2011), and only a few studies have investigated the axial compressive behavior of square and rectangular CFFTs (Mirmiran et al. 1998; Hong and Kim 2004; Fam et al. 2005; Ozbakkaloglu and Oehlers 2008a).

Very much like that of FRP, the popularity of high-strength concrete (HSC) in the construction industry has been on a steady incline during the last two decades. It is now understood that HSC offers superior performance and economy over normal-strength concrete (NSC) when used in the construction of bridges and multi-story buildings. The use of HSC for CFFTs is attractive because the combination of two high-strength materials (i.e., HSC and FRP) leads to high-performance columns. The tests conducted by Ozbakkaloglu and Saatcioglu (2006, 2007) on large-scale HSCFFT columns have demonstrated the ability of these columns to exhibit highly ductile behavior under simulated seismic loading. However, research on the compressive behavior of FRP-confined HSC, in general, and on HSCFFT, in particular, has so far been extremely limited, with only a handful of studies reported on FRP-wrapped HSC cylinders (Rousakis 2001; Berthet et al. 2005; Mandal et al. 2005; Almusallam 2007; Eid et al 2009; Wu et al. 2009; Cui and Sheikh 2010; Xiao et al. 2010; Ozbakkaloglu and Akin 2011) and just one on FRP-wrapped HSC specimens with square cross-sections (Wang and Wu 2010). This review of the literature clearly demonstrates that the lack of experimental studies forms a major impediment to clear understanding of the axial compressive behavior of HSCFFTs.

As the first experimental study reported in the literature on the axial compressive behavior of square and rectangular HSCFFTs, this paper presents the results a test program which was aimed at investigating the influence of critical confinement parameters on the performance of square and rectangular HSCFFTs. The results of the experimental program are first presented, followed by a discussion on the influence of the main test parameters on the test results.

EXPERIMENTAL PROGRAM

Test Specimens and Materials

A total of 24 square and rectangular HSCFFTs were manufactured and tested under axial compression. Details of the test specimens are shown in Table 1. All of the specimens were 300 mm in height. The cross-sectional dimensions were measured at the concrete core, and were chosen such that the ratio of the sectional area (A) to the perimeter of the section (S) would be equal in square and rectangular specimens to maintain a constant FRP reinforcement ratio (ρ) among specimens with different sectional aspect ratios.

$$\rho = \frac{S \cdot t}{A} \tag{1}$$

where t = total nominal fiber thickness of the FRP tube. The test parameters included: the aspect ratio of the specimen cross-section (i.e., h/b = 1.0, 1.5 or 2.0), thickness of the FRP tube (i.e., 3 or 5 layers), and corner radius of the FRP tube (i.e., R =15 mm or 30 mm).

The specimens were prepared using a single HSC mix design, which developed an average unconfined concrete compressive strength of 77.9 MPa during the period of testing. The mix consisted of crushed bluestone as the coarse aggregate with a nominal maximum size of 10 mm, and silica fume added at 8 percent of the binder content by weight. The specimens were cast of four separate batches with the same mix proportions. The testing of the specimens started right after the attainment of the 28-day strength and continued for approximately 2 weeks. The changes in the strength of unconfined concrete were monitored by cylinder tests conducted throughout the testing program. The cylinder strengths of unconfined concrete f'_c at the day of testing are reported together with the corresponding axial strains ε_{co} in Table 1 for each concrete batch. ε_{co} values were not measured directly for all the control specimens but were calculated using the expression given by Tasdemir (1998). As can be seen in Table 1, the average test day cylinder strengths of these batches varied between 76.6 and 79.6 MPa.

The FRP tubes were prepared using a manual wet lay-up process by wrapping epoxy resin impregnated carbon fiber sheets around precision-cut high-density Styrofoam templates in the hoop direction. An overlap length of 100 mm was provided in all specimens to prevent premature debonding failure. The FRP tubes with 3 layers of FRP were wrapped with a single FRP sheet continuously, whereas the tubes having 5 layers of FRP were wrapped by two FRP sheets, and hence had two overlap regions. The CFFTs before testing are shown in Fig.1. The details of the test specimens are given in Table 1 and the properties of the unidirectional carbon fiber sheets used in the manufacturing of the FRP tubes are provided in Table 2. The test results from the FRP coupon specimens prepared using the 0.117 mm thick version of the same carbon fiber sheets were previously reported in Ozbakkaloglu and Oehlers (2008b), and they are in close agreement with the fiber properties reported in table 2. Two nominally identical specimens were tested for each unique specimen configuration.

Specimen Designation

The specimens in Table 1 were labeled as follows: letters A, R and L were used to represent the test parameters, namely the sectional aspect ratio, corner radius, and number of FRP layers, respectively. Each letter was followed by a number that was used to represent the value of that particular parameter for a given specimen. Finally, the last number in the specimen designation (i.e., 1 or 2) was used to make distinction between two nominally identical specimens. For instance, A15R30L3-1 is the first of the two identical specimens that had a sectional aspect ratio of 1.5, corner radius of 30 mm and 3 layers of FRP.

Instrumentation and testing

Axial deformations of the specimens were measured with four linear variable displacement transducers (LVDTs), which were mounted at the corners between the loading and supporting

steel plates of the compression test machine as shown in Fig.2. The recorded deformations were used in the calculation of the average axial strains along the height of the specimens. In addition, half of the specimens (i.e., one of the two nominally identical specimens) were instrumented at the mid-height with two unidirectional strain gauges with a gauge length of 20 mm to measure axial strains, which were used to validate LVDT measurements at the early stages of loading. Transverse strains were measured by six unidirectional strain gauges that were installed at the mid-height on the FRP tube. Four of these gauges were installed at the mid-span of each face of the specimen and they had a gauge length of 20 mm. The remaining two gauges were installed on opposite corners of the specimens and had a gauge length of 10 mm.

The specimens were tested under axial compression using a 5000 kN capacity universal testing machine. During the initial elastic stage of the behavior, the loading was applied with load control at 3 kN per second, whereas displacement control was used at approximately 0.01 mm per second beyond the initial softening until specimen failure. Prior to testing, all specimens were capped at both ends to ensure uniform distribution of the applied pressure, and the load was applied directly to the concrete core.

TEST RESULTS AND DISCUSSION

Failure mode

The typical failure modes of the test specimens are shown in Fig. 3. All of the specimens failed by the rupture of the FRP tube at or near one of the corners of the specimen. In the majority of the specimens the rupture of the FRP tubes happened at the mid-height of the specimen. A few of the specimens had failure regions that extended from the mid-height of the specimen to one of its ends.

Ultimate condition

The ultimate condition of FRP-confined concrete is often characterized as the ultimate strength and axial strain of concrete recorded at the rupture of the FRP jacket. This makes the relationship between the ultimate strength f'_{cc}, ultimate axial strain ε_{cu} and hoop rupture strain $\varepsilon_{h,rup}$ an intimate one. Axial stress and strain data of the test specimens are reported in Table 3, and the FRP hoop rupture strains recorded on the specimens are given in Tables 3 and 4.

Axial stress and strain

The summary of the key experimental results are shown in Table 3, which include: the ultimate axial strength and strain of the specimens (f'_{cc} *and* ε_{cu}), the axial stress that corresponds to the point of transition from the initial ascending branch to the second branch of the stress-strain curve (f'_{ct}), and the strength and strain enhancement ratios (f'_{cc}/f'_{c} *and* $\varepsilon_{cu}/\varepsilon_{co}$). The ultimate confined-concrete strengths f'_{cc} were calculated from the recorded axial loads just prior to the failure of the specimens. The ultimate axial strain of confined concrete ε_{cu} was averaged from the four LVDTs. A closer inspection of the results reported in Table 3 reveals that transition stresses f'_{ct} of some of the specimens were slightly lower than the cylinder strengths of the unconfined concrete f'_{c} used in these specimens. As previously discussed in Ozbakkaloglu and Saatcioglu (2004), this seemingly unexpected observation can be explained by slight differences observed between the strength of concrete in structural members and the cylinder strength of the same concrete, as caused by differences in size, shape, curing conditions and casting practice. It follows, therefore, that for the specimens of the present study the strength of the unconfined concrete inside the FRP tubes was slightly lower than the strength obtained for the same concrete from the cylinder tests.

The results reported in Table 3 illustrate that the ultimate strength f'_{cc} of the specimens increase with an increase in corner radius and decrease with an increase in sectional aspect ratio. These observations were expected and are in agreement with those reported previously on FRP-confined NSC specimens (Rochette and Labossiere 2000; Ozbakkaloglu and Oehlers 2008a; Wang and Wu

2008; Wu and Wei 2010). Comparison of the specimens having the same number of FRP layers and corner radius indicate that, in general, an increase in sectional aspect ratio leads to a decrease in the ultimate strain ε_{cu}. Again, this observation is in agreement with those made by Wu and Wei (2010). However, Table 3 illustrates that this influence is not as clear from the comparison of the specimens with aspect ratios of 1.5 and 2.0 as the one that can be observed from the comparison of the specimens with aspect ratios of 1.0 and 1.5. Another interesting observation from Table 3 is that an increase in the tube corner radius results in a decrease in the ultimate strain of the specimens. As can be seen in Table 3, this trend is consistent in every specimen pair of the present study, independent of the tube thickness and sectional aspect ratio of the specimens. The results reported in Table 3 also show that, as expected, both the ultimate strength f'_{cc} and strain ε_{cu} increase with increased number of FRP layers. Influence of these key confinement parameters on the stress-strain behavior of the specimens is discussed in detail later in the paper.

Hoop strains

Table 4 presents the recorded hoop rupture strains $\varepsilon_{h,rup}$ and calculated strain reduction factors k_ε (Eq.2) for the test specimens. It has been discussed previously in a number of studies (e.g., Pessiki et al. 2001; Ilki and Kumbasar 2003; Lam and Teng 2003, 2004; Ozbakkaloglu and Akin 2011) that the ultimate hoop strain $\varepsilon_{h,rup}$ reached in the FRP jacket is often smaller than the ultimate tensile strain of the fibers ε_{fu}, which necessitates the use of a strain reduction factor k_ε in the determination of the actual confining pressures.

$$k_\varepsilon = \frac{\varepsilon_{h,rup}}{\varepsilon_{fu}} \tag{2}$$

Furthermore, unlike in circular sections, concrete in FRP-confined square and rectangular sections is not subjected to nearly uniform confining pressure, and the pressure provided by the FRP tube varies around the perimeter of the cross-section. To provide some insight into the distribution of the hoop strains around the perimeter of the square and rectangular CFFTs at

ultimate, in Table 4 the average hoop rupture strains and resulting strain reduction factors obtained from the strain gauges placed on the corners, long-spans and short-spans of the specimens are reported separately. The overall average strain reduction factor k_ε was calculated as 0.48 for the specimens of the present study based on the readings obtained from the six hoop strain gauges placed on each specimen. It was found that strain reduction factor was not sensitive to the aspect ratio, with the average values of k_ε calculated as 0.51, 0.46 and 0.47, respectively, for the specimens having aspect ratios of 1.0, 1.5 and 2.0. However, as evident from Table 4, for the majority of the specimens the strain reduction factors showed significant variations around the perimeter of the specimen, with average values calculated for the short-spans ($k_{\varepsilon-short}$), long-spans ($k_{\varepsilon-long}$) and corners ($k_{\varepsilon-corner}$) as 0.59, 0.48 and 0.36, respectively.

To illustrate the influence of the sectional aspect ratio and corner radius on the strain reduction factor, average values of the strain reduction factors are established and presented in Table 5. Closer inspection of the results reported in Table 5 leads to two important observations on i) the influence of corner radius on the development of corner strains, and ii) the influence of sectional aspect ratio on the development of short- and long-span strains. As can be seen Table 5, the average value of $k_{\varepsilon-corner}$ was 0.31 and 0.40, respectively, for the specimens with 15 mm and 30 mm corner radius. This indicates that increased corner radius leads to an increase in the corner strains, which in turn leads to a more uniform hoop strain distribution around the perimeter of the specimen. It is understood that the confinement effectiveness of FRP tubes improves with the uniformity of the confining pressure (Lam and Teng 2003; Ozbakkaloglu and Oehlers 2008b), and hence the above observations suggest that the tubes with well-rounded corners provide more effective confinement. This conclusion is in agreement with those can be drawn from the results of the axial compression tests discussed in the following section.

The results reported in Table 5 also illustrate that the average hoop strain reduction factors were higher on the short-spans of the rectangular specimens ($k_{\varepsilon-short}$) than their long-spans ($k_{\varepsilon-long}$), and the difference became more significant as the sectional aspect ratio increased. These results indicate that an increase in the aspect ratio leads to an increase in $k_{\varepsilon-short}$ and a decrease in $k_{\varepsilon-long}$. The average $k_{\varepsilon-short}$ /$k_{\varepsilon-long}$ ratio of the specimens with an aspect ratio of 1.5 was calculated as 1.29, whereas the same ratio was equal to 1.63 for the specimens with an aspect ratio of 2.0. This increase in the $k_{\varepsilon-short}$ /$k_{\varepsilon-long}$ ratio leads to a less uniform confining pressure distribution and thereby results in reduced effectiveness of the confining tube. This conclusion is also in agreement with the axial compression test results discussed in the next section.

Another observation from the results given in Tables 4 and 5 is that the change in corner radius had no noticeable influence on the distribution of hoop strains between the short- and long-spans of the specimens. Likewise, the results reported in Table 4 indicate that the number of FRP layers did not have any major influence either on the average value or on the distribution of the hoop rupture strains within the range of confinement levels investigated in this study. That is, the aforementioned observations on the influences of corner radius and sectional aspect ratio were equally applicable to the specimens with 3 and 5 layers of FRP, and the average value of k_{ε} was 0.48 for both series.

Axial stress-strain behavior

Figure 4 illustrates the different stages observed on a typical axial stress-train curve of the specimens of the present study. The notation and definitions introduced in Fig.4 are used consistently thought the discussion presented in this section. Axial stress-strain curves of all the test specimens are shown in Figs. 5 to 7. The curves of the companion specimens shown in Figs. 5 and 6 were represented through the use of two different line styles. It is evident from Figs. 5-7 that sufficiently confined square and rectangular HSCFFTs can exhibit highly ductile

compressive behavior. However, the figures also illustrate that both the amount, as determined by the number of FRP layers, and effectiveness of confinement, as determined by the corner radius and sectional aspect ratio, play a crucial role on the axial compressive behavior of HSCFFTs. It is well established that FRP-confined concrete exhibits a monotonically ascending curve, which consists of a parabolic first portion and a nearly straight-line second portion, if the level of confinement exceeds a certain threshold (Lam and Teng 2003; Ozbakkaloglu and Oehlers 2008a). On the other hand, when the confinement level is below this threshold the first ascending branch is followed by a descending branch after the transition point. In the present paper, the term 'sufficient confinement' is used to refer to this theoretical threshold confinement level, the presence of which results in a stress-strain curve with an almost horizontal second branch without any strong tendency to ascend or descend. The level of confinement provided by square and rectangular tubes is dependent not only on the amount of confinement but also on the effectiveness of confinement. In this context, the term confinement effectiveness is being used to establish a relationship between the amount and level of confinement. It is known that circular CFFTs provide the highest possible confinement effectiveness (i.e. 100%), whereas the confinement effectiveness of the square and rectangular CFFTs are lower and it varies as a function of the corner radius and sectional aspect ratio. These influences are discussed in the following sections.

As illustrated in Figs. 5-7, all of the three aforementioned stress-strain curve types were observed for the specimens of the present study, with the majority of the specimens exhibiting either descending or almost horizontal second branches. As expected, the stress-strain behavior of the specimens along the second branch is influenced significantly by the important confinement parameters, including the corner radius, sectional aspect ratio and number of FRP layers. It can be observed in Figs. 5-7 that most of the specimens experienced a sudden drop in strength starting right at the transition point on their stress-strain curves. This phenomenon, which is referred to

herein as 'initial strength softening', can be associated to the brittle nature of the higher strength concretes. During this stage of the stress-strain behavior, the hoop strains recorded on the FRP tube of the specimens increased rapidly and at one point confining pressures generated by the FRP tube reached to a level that was high enough to sufficiently confine the HSC. This point corresponds to the plateau formation on the stress-strain curves shown in Figs. 5-7, which follows the initial strength softening region. Beyond this point, further increase in the axial strains lead either to an almost flat or a slightly ascending type of final portion in the stress-strain curves of the test specimens, as illustrated in Figs. 5-7. The idealized trends of the second branches of the stress-strain curves can be defined through the use of an ultimate strength to transition stress ratio (f'_{cc}/f_{ct}). This ratio is calculated for each test specimen and the average ratios for each series are reported in Table 3, where a value greater than 1.0 indicates an overall ascending type of second branch and lower than 1.0 an overall descending type. The influence of the key confinement parameters on the stress-strain behavior of square and rectangular HSCFFTs is discussed in the following sections.

Effect of corner radius

Figure 5 illustrates the influence of the corner radius on the axial stress-strain curves for the specimens of the present study. It can be seen from the figure that, in general, the corner radius of the FRP tube has a significant influence on the trend of the second branch of the stress-strain curves that follows the initial ascending branch. The complete trend of the second branch can be defined through the investigation of the two previously discussed regions that form this branch (Fig. 4). The magnitude of strength loss observed along the ‘initial strength softening’ region and the slope of the ‘final portion of the curve’ that follows the softening region are the two main quantities required to establish the complete trend of the second branch. The results of the present study indicate a strong correlation between the confinement effectiveness of the FRP, as influenced by corner radius and sectional aspect ratio, and the magnitude of the strength loss

observed at the point of transition. As evident from Fig. 5, the specimens with 30 mm corners experienced a lower strength drop at the transition point compared to the specimens with 15 mm corners. The difference was particularly pronounced for the specimens with aspect ratios of 1.0 and 1.5 where the initial strength drop was less significant compared to the specimens with an aspect ratio of 2.0. This suggests that the increase in the confinement effectiveness attained as a result of rounding the corners was sufficient to reduce the initial strength loss of series A10 and A15 specimens. On the other hand apart from a single specimen (i.e., A20R30L5-1) it was not possible to prevent or reduce the strength drop observed in A20 series specimens through better rounding of their corners. This implies that increased aspect ratio resulted in a large reduction in the confinement effectiveness of these specimens, which could not be recovered sufficiently through increased corner radius.

Figure 5 also illustrates that increase in the corner radius, in general, leads to an increase in the slope of the final portion of the stress-strain curves that follow the initial strength softening region. Similar observation were previously reported for FRP-confined NSC (Rochette and Labossiere 2000; Ozbakkaloglu and Oehlers 2008a; Wang and Wu 2008). In contrast to its aforementioned beneficial influences on the stress-strain behavior, however, as evident from Table 3 and Fig.5, an increase in corner radius resulted in a decrease in the ultimate axial strains of the specimens. In particular, the comparison of the stress-strain curves for the A10L5 series specimens shown in Fig. 5(b) suggests that for CFFTs designed with sufficiently high amount and effectiveness of confinement, a CFFT with a smaller corner radius might exhibit a more favorable stress-strain behavior (i.e., with an almost flat and long second branch) compared to a CFFT with a larger corner radius (i.e., with an ascending but short second branch). This observation points to the importance of understanding the interaction between the key confinement parameters that influence the behavior of square and rectangular CFFTs to design these systems effectively for a desired level of performance.

Effect of tube thickness

Figure 6 illustrates the effect of FRP tube thickness on the axial stress-strain behavior of the CFFTs of the present study. The specimens shown in each of Figs. 6(a) to 6(f) were confined with either 3 or 5 layers of FRP, and were identical except for the amount of confinement. As expected, the stress-strain curves shown in Fig.6 and the $\varepsilon_{cu}/\varepsilon_{co}$ ratios given in Table 3 illustrate that the ultimate axial strain of the specimens is influenced significantly and increase directly with increased tube thickness. On the other hand, the results shown in the same table and figure also indicate that the relationship between the tube thickness and the ultimate concrete strength is not as straightforward. Figure 6 shows that the influence of the tube thickness on the overall trend of the second part of the stress-strain curve is dependent on the confinement effectiveness of the tube. As evident from the stress-strain curves of A20R15 series specimens shown in Fig. 6(e), the tube thickness has only a minor influence on the trend of the second portion of the stress-strain curve when the confinement effectiveness of the CFFT is low. As a result, the thickness of the FRP tube only marginally influences the ultimate strength of the CFFTs with low confinement effectiveness. On the other hand, when the confinement effectiveness of the FRP tube is high and the CFFT exhibits a stress-strain curve with an ascending second branch, the tube thickness has a direct influence on the ultimate strength of the CFFTs, as was observed for A10R15 and A10R30 series specimens shown in Figs. 6(a) and 6(b), respectively. The aforementioned observations are consistent with those reported in Ozbakkaloglu and Oehlers (2008a) for NSCFFTs. The examination of the stress-train curves shown in Fig.6 also reveal that the thickness of the FRP tube plays only a marginal role on the initial strength loss experienced by the specimens of the present study. This region appears to be more sensitive to the parameters that influence the effectiveness of confinement (i.e., corner radius and aspect ratio) than its amount.

Effect of sectional aspect ratio

Figure 7 presents the comparison of the axial stress-strain behavior of the specimens with different sectional aspect ratios. The specimens shown in each of Figs. 7(a) to 7(h) had the same corner radius and nearly identical concrete strengths and FRP reinforcement ratios as reported in Table 1. It is clear from the stress-strain curves shown in Fig. 7 that the magnitude of the initial strength softening experienced by the specimens was influenced greatly by their sectional aspect ratios, and the strength loss at the point of transition increased with an increase in the aspect ratio. As illustrated in Fig.7, this observation is independent of the tube thickness and the corner radius of the specimens, and is equally applicable for all series of specimens of the present study. As discussed previously, there is a strong correlation between the confinement effectiveness and the magnitude of the initial strength loss, and hence the above observation suggests that the confinement effectiveness of CFFTs decreases with increased sectional aspect ratio. Similar observations were reported for FRP-confined NSC by a number of previous studies (Lam and Teng 2003, Ozbakkaloglu and Oehlers 2008a; Wu and Wei 2010). However, the aforementioned reduction in the confinement effectiveness appears to be having a more significant detrimental effect on the behavior of HSCFFTs compared to NSCFFTs. The increased sensitivity of the higher strength concretes to confinement effectiveness can be explained by the more sudden and brittle failure mode of HSC compared to the gradual failure mode of NSC, which exhibits a more pronounced softening behavior and in turn allows the gradual activation of the confinement mechanism. Another interesting observation from Fig.7 is that the slope of the final portion of the stress-strain curves, the part that follows the 'initial strength softening' region, does not appear to be affected significantly by the sectional aspect ratio. This observation is not in agreement with those can be drawn from the previous studies reported on FRP-confined NSC (Lam and Teng 2003, Ozbakkaloglu and Oehlers 2008a; Wu and Wei 2010) where the influence of the aspect ratio on the slope of the second portion of the stress-strain relationship was rather pronounced. On the other hand, if an overall trend for the part of the stress-strain curve that is beyond the transition point is defined through the use of f'_{cc}/f_{ct} ratios discussed previously, the influence of

the aspect ratio on these trends agrees well with those reported for FRP-confined NSC in the aforementioned studies.

CONCLUSIONS

This paper has presented the results of an experimental study on the behavior of square and rectangular HSCFFTs under axial compression. Based on the results and discussions presented in the paper the following conclusions can be drawn:

1. Sufficiently confined square and rectangular HSCFFTs can exhibit highly ductile compressive behavior. However, the behavior of HSCFTTs is highly sensitive to the effectiveness of confining tube, and tubes with low confinement effectiveness may not provide sufficient confinement to allow HSCFFTs to maintain their load carrying capacity after their initial peak strengths are attained.
2. Confinement effectiveness of FRP tubes increases with an increase in corner radius and decreases with an increase in sectional aspect ratio. Both of these parameters significantly influence the overall trend of the second portion of the stress-strain relationship of HSCFFTs. Increased corner radius improves the overall trend of this region but it may result in a reduced ultimate axial strain. An increase in sectional aspect ratio may also lead to a decrease in the ultimate strain.
3. FRP tube thickness has a significant influence on the ultimate strain of HSCFFTs, and the ultimate strain increases with the tube thickness. Although the tube thickness has a significant effect on the length of the second branch of the stress-strain curve, it only has a minor influence on the trend of this part of the curve when the confinement effectiveness of the tube is low. Therefore, increased tube thickness results in an increase in the ultimate strength of HSCFTTs only if the confinement effectiveness of the tube is sufficiently high.

4. Rectangular HSCFFTs develop higher hoop strains along their short-spans than their long-spans at ultimate. The ratio of the short-to-long span strains increase with an increase in the aspect ratio.
5. HSCCFTs with well-rounded corners develop higher corner hoop strains at ultimate compared to HSCFFTs with smaller corner radius.
6. For the range of confinement levels investigated in this study, FRP tube thickness does not appear to have any major influence neither on the average value or on the distribution of the hoop rupture strains recorded on HSCFFTs.

ACKNOWLEDGEMENTS

The author would like to thank Ms. Clarke and Messrs. Cuts, Schleuniger and Sitaras, who have undertaken the tests reported in this paper as part of their undergraduate theses. This research is part of an ongoing programme at The University of Adelaide on FRP-concrete composite columns.

REFERENCES

Almusallam, T. H. (2007). “Behaviour of normal and high-strength concrete cylinders confined with E-Glass/Epoxy composite laminates.” *Composites Part B-Engineering*, 38(5-6), 629-639.

Berthet, J. F., Ferrier, E., and Hamelin, P. (2005). “Compressive behaviour of concrete externally confined by composite jackets. Part A: Experimental study.” *Construction and Building Materials, Elsevie*r, 19, 223-232.

Chaallal, O., Hassan, M., Shahawy, M. (2003). “Confinement model for axially loaded short rectangular columns strengthened with fiber reinforced polymer wrapping.” ACI Struct J 2003; 100(2): 215–21.

Cui, C., and Sheikh, S.A. (2010). “Experimental study of normal- and high-strength concrete confined with fiber-reinforced polymers.” *Journal of Composites for Construction, ASCE*, 14(5), 553-561.

Dai, J.G., Bai, Y.L., and Teng, J.G. (2011). “Behavior and modeling of concrete confined with FRP composites of large deformability.” J. Compos. Constr., 15(6), 963-973."

De Lorenzis, L., and Tepfers, R. (2003). “Comparative Study of Models on Confinement of Concrete Cylinders with Fiber-Reinforced Polymer Composites.” Journal of Composites for Construction, ASCE, 7, 3, pp 219-237.

Eid, R., Roy, N., and Paultre, P. (2009). “Normal- and high-strength concrete circular elements wrapped with FRP composites.” *Journal of Composites for Construction, ASCE*, 13(2), 113-124.

Fam, A. Z., and Rizkalla, S. H. (2001). “Behavior of Axially Loaded Concrete-Filled Circular Fiber-Reinforced Polymer Tubes.” ACI Structural Journal, 98, 3, pp 280-289.

Fam, A. Z., and Rizkalla, S. H. (2002). “Flexural behavior of concrete-filled fiber reinforced polymer circular tubes.” *Journal of Composites for Construction*, 6(2), 123-132.

Fam, A., Schnerch, D. and Rizkalla, S. (2005). "Rectangular Filament-Wound GFRP Tubes Filled with Concrete under Flexural and Axial Loading: Experimental Investigation." Journal of Composites for Construction, ASCE, Vol. 9, No. 1, pp 25-33.

Hadi, M. N. S. (2006) “Behaviour of FRP wrapped normal strength concrete columns under eccentric loading.” J. Compos. Struct., 2006. **72**(4): p. 503-511.

Hong, W.K., and Kim, H.C. (2004). “Behavior of concrete columns confined by carbon composite tubes”, Canadian Journal of Civil Engineering, 31(2), pp 178–188.

Ilki, A., and Kumbasar, N. (2003). "Compressive behavior of carbon fiber composite jacketed concrete with circular and non-circular cross sections." *Journal of Earthquake Eng.*, 7(3), 381–406.

Ilki A, Peker O, Karamuk E, Demir C, Kumbasar N. (2008). “FRP retrofit of low and medium strength circular and rectangular reinforced concrete columns.” J. Mater Civ Eng, ASCE; 20(2): 169-88.

Lam, L., and Teng, J.G. (2003). “Design-oriented stress-strain model for FRP-confined concrete in rectangular columns.” Journal of Reinforced Plastics and Composites, 22(13), 2003, pp 1149–1186.

Lam, L., and Teng, J. G. (2004). “Ultimate condition of fiber reinforced polymer-confined concrete.” *Journal of Composites for Construction, ASCE*, 8(6), 539-548.

Li., G. (2006). “Experimental study of FRP confined concrete cylinders.” Engineering Structures, Vol. 28, pp 1001-1008.

Mandal., S., Hoskin., A., and Fam., A. (2005). “Influence of Concrete Strength on Confinement Effectiveness of Fiber-Reinforced Polymer Circular Jackets.” ACI Structural Journal, 102, 3, pp 383-392.

Mastrapa, J. C. (1997). “Effect of construction bond on confinement with fiber composites.” MS thesis, Univ. of Central Florida, Orlando.

Mirmiran, A., Samaan, M., Cabrera, S., and Shahawy, M. (1998). “Design, manufacture, and testing of a new hybrid column.” Constr. Build. Mater.12 (1), 39-49.

Mirmiran, A., Shahawy, M., and Beitleman, T. (2001). “Slenderness Limit for hybrid FRP-concrete columns.” Journal of Composites for Construction, ASCE, 5, 1, pp 26-34.

Mirmiran, A., Shahawy, M., Samaan, M., El Echary, H., Mastrapa, J.C., and Pico, O. (1998). “Effect of Column Parameters on FRP-confined Concrete.” Journal of Composites for Construction, ASCE, 2, 4, pp 175-185.

Mohamed, H., and Masmoudi, R. (2010) “Axial Load Capacity of Concrete-Filled FRP Tube Columns: Experimental versus Predictions.” J. Compos. Constr., ASCE, 14(2): p. 231-243.

Moss, R. M. (2001). “Behavior of large diameter column reinforced with wrapped glass fibre reinforced plastic tubing.” The Structural Engineer, 79, 14, pp 23-31.

Ozbakkaloglu, T., and Akin, E. (2011) “Behavior of FRP-confined normal- and high-strength concrete under cyclic axial compression.” Journal of Composites for Construction, ASCE, 10.1061/(ASCE)CC.1943-5614.0000273

Ozbakkaloglu, T., and Oehlers, D. J. (2008a). “Concrete-filled Square and Rectangular FRP Tubes under Axial Compression.” Journal of Composites for Construction, ASCE, Vol.12, No.4, pp.469-477.

Ozbakkaloglu, T. and Oehlers, D. J. (2008b). “Manufacture and testing of a novel FRP tube confinement system.” *Engineering Structures*, 30, 2448-2459.

Ozbakkaloglu, T., and Saatcioglu., M. (2004). “Rectangular Stress Block for High-Strength Concrete.” ACI Structural Journal, V. 101, No. 4, pp. 475-483.

Ozbakkaloglu, T., and Saatcioglu, M. (2006). “Seismic behavior of high-strength concrete Columns confined by fiber reinforced polymer tubes.” *Journal of Composites for Construction, ASCE*, 10(6), 538-549.

Ozbakkaloglu, T., and Saatcioglu, M. (2007). “Seismic performance of square high-strength concrete columns in FRP stay-in-place formwork.” *Journal of Structural Engineering, ASCE*, 133(1), 44-56.

Ozcan, O., Binici, B., Ozcebe, G. (2010). “Seismic strengthening of rectangular reinforced concrete columns using fiber reinforced polymers.” Eng Struct; 32(4): 964–73.

Park, J. H., Jo, B. W., Yoon, S. J., and Park, S. K. (2011). “Experimental investigation on the structural behavior of concrete filled FRP tubes with/without steel re-bar.” KSCE J. Civ. Eng., 15(2): p. 337-345.

Pessiki, S., Harries, K. A., Kestner, J. T., Sause, R. and Ricles, J. M. (2001). “Axial behavior of reinforced concrete columns confined with FRP jackets.” *Journal of Composites for Construction, ASCE*, 5(4), 237-245.

Rochette, P., and Labossiere, P. (2000). “Axial Testing of Rectangular Column Models Confined with Composites.” Journal of Composites for Construction, ASCE, 4, 3, pp 129-136.

Rousakis, T.C. (2001). “Experimental investigation of concrete cylinders confined by carbon FRP sheets under monotonic and cyclic axial compression load.” *Research Report 01:2*, Division of Building Technology, Chalmers University of Technology.

Saafi, M., Toutanji H.A., Li, Z. (1999). “Behavior of Concrete Columns Confined with Fiber Reinforced Polymer Tubes.” ACI Structural Journal, 96, 4, pp 500-509.

Saatcioglu, M., Ozbakkaloglu, T., Elnabelsy, G. (2008) “Seismic behavior and design of reinforced concrete columns confined with FRP stay-in-place formwork.” ACI SP257, p. 149-170.

Seible F, Karbhari VM, Burgueno R. (1999). “Kings stormwater channel and I-5/Gilman bridges, USA.” Journal of the International Association for Bridge and Structural Engineering (IABSE), Structural Engineering International; 9(4):250–3.

Shao, Y., and Mirmiran, A. (2005). “Experimental Investigation of Cyclic Behavior of Concrete-Filled FRP Tubes,” Journal of Composites for Construction, ASCE, 9(3), 263-273.

Tasdemir, M. A., Tasdemir, C., Jefferson, A. D., Lydon, F. D., and Barr, B. I. G. (1998). “Evaluation of strains at peak stresses in concrete: a three-phase composite model approach.” *Cem. Concr. Res.*, 20(4), 301-18.

Tegola, A. L., and Manni, O. (1999). “Experimental investigation on concrete confined by fiber reinforced polymer and comparison with theoretical model”, ACI SP-188, pp 243-254.

Wang, L. M., and Wu, Y. F. (2008). “Effect of Corner Radius on the Performance of CFRP-Confined Square Concrete Columns: Test.” Eng. Struct., 30(2): p. 493-505.

Wang, Y.F., Wu, H.L. (2010). “Experimental investigation on square high-strength concrete short columns confined with AFRP sheets.” J Compos Constr, ASCE; 14(3): 346–51.

Wu, H. L., Wang, Y. F., Yu, L., and Li, X. R. (2009). “Experimental and computational studies on high-strength concrete circular columns confined by aramid fiber-reinforced polymer sheets.” *Journal of Composites for Construction, ASCE*, 13(2), 125-134.

Wu Y.F., and Wei Y.Y. (2010). “Effect of cross-sectional aspect ratio on the strength of CFRP-confined rectangular concrete columns.” Eng Struct; 32: 32-45.

Xiao, Q. G., Teng, J. G., and Yu, T. (2010). “Behavior and modeling of confined high-strength concrete.” *Journal of Composites for Construction, ASCE*, 14(3), 249-259.

Xiao, Y., and Wu, H. (2000). “Compressive behavior of concrete confined by carbon fiber composite jackets.” *J. Mater. Civil Eng.*, ASCE, 12(2), 139-46.

Yamakawa, T., Zhong, P., and Ohama, A. (2003). “Seismic Performance of Aramid Fiber Square Tubed Concrete Columns with Metallic and/or Non-metallic Reinforcement” Journal of Reinforced Plastics and Composites, 22, 13, pp 1221-1237.

Zaghi, A.E., Saiidi, M.S., and Mirmiran, A. (2012). “Shake table response and analysis of a concrete-filled FRP tube bridge column.” Composite Structures, 94 (5), 164-1574.

Zhu, Z., Ahmad, l., and Mirmiran, A. (2005). “Effect of column parameters on axial compression behavior of concrete-filled FRP tubes.” Advances in Structural Engineering, 8, 4, pp 443-449.

Table 1. Properties of test specimens

Concrete batch	f'_c (MPa)	ε_{co} (%)	Specimen	b (mm)	h (mm)	Number of FRP layers (L)	Corner radius (R) (mm)	FRP reinforcement ratio (ρ) (%)
1	76.6	0.295	A10R15L3-1	150	150	3	15	1.81
			A10R15L3-2					
			A10R30L3-1				30	1.78
			A10R30L3-2					
			A10R15L5-1			5	15	3.02
			A10R15L5-2					
2	77.2	0.296	A10R30L5-1				30	2.97
			A10R30L5-2					
			A15R15L3-1	125	187.5	3	15	1.82
			A15R15L3-2					
			A15R30L3-1				30	1.78
			A15R30L3-2					
3	79.6	0.301	A15R15L5-1			5	15	3.03
			A15R15L5-2					
			A15R30L5-1				30	2.97
			A15R30L5-2					
			A20R15L3-1	112.5	225	3	15	1.82
			A20R15L3-2					
4	78.2	0.298	A20R30L3-1				30	1.79
			A20R30L3-2					
			A20R15L5-1			5	15	3.04
			A20R15L5-2					
			A20R30L5-1				30	2.99
			A20R30L5-2					

Table 2. Properties of fiber sheets as provided by the manufacturer

Type	Nominal thickness t_f (mm/ply)	Tensile strength f_{fu} (MPa)	Ultimate Tensile Strain ε_{fu} (%)	Elastic Modulus E_f (GPa)	Weight (g/m^2)
Carbon	0.234	3800	1.55	240	400

Table 3. Test results

Specimen	f'_{ct} (MPa)	f'_{cc} (MPa)	ε_{cu} (%)	$\varepsilon_{h,rup}$ (%)	f'_{co}/f'_{ct}	$\varepsilon_{cu}/\varepsilon_{co}$	k_ε
A10R15L3-1	78.0	73.6	2.30	0.80	0.89	7.3	0.56
A10R15L3-2	77.5	65.2	2.03	0.95			
A10R30L3-1	86.7	83.3	1.59	0.78	0.96	5.2	0.51
A10R30L3-2	84.4	80.5	1.47	0.80			
A10R15L5-1	79.4	88.5	3.36	0.67	1.05	10.7	0.46
A10R15L5-2	80.6	78.7	2.94	0.76			
A10R30L5-1	94.6	114.2	2.13	0.86	1.21	7.0	0.51
A10R30L5-2	86.4	104.7	1.99	0.72			
A15R15L3-1	80.7	55.1	1.50	0.77	0.71	5.0	0.45
A15R15L3-2	79.1	58.6	1.48	0.63			
A15R30L3-1	85.5	77.1	1.33	0.76	0.97	4.2	0.41
A15R30L3-2	74.9	77.1	1.17	0.52			
A15R15L5-1	85.5	73.9	1.96	0.56	0.88	7.5	0.47
A15R15L5-2	84.7	75.1	2.55	0.90			
A15R30L5-1	92.7	95.9	1.48	0.68	1.05	5.4	0.49
A15R30L5-2	90.1	95.7	1.76	0.84			
A20R15L3-1	76.3	42.3	1.84	0.61	0.60	5.8	0.44
A20R15L3-2	78.6	51.1	1.63	0.75			
A20R30L3-1	74.4	55.7	1.53	0.77	0.75	5.0	0.51
A20R30L3-2	82.4	62.1	1.44	0.80			
A20R15L5-1	77.5	63.5	2.13	0.74*	0.74	6.3	0.43
A20R15L5-2	84.9	55.5	1.60	0.59			
A20R30L5-1	85.7	89.6	1.99	0.86	1.01	6.0	0.50
A20R30L5-2	79.0	77.3	1.57	0.70			

*One of the corners strain gauges were excluded from the calculation of the average hoop rupture strain.

Table 4. Recorded hoop strains and calculated strain reduction factors

Specimen	$\varepsilon_{h,rup}$ (%)			k_{ε}		
	Corner	Long-span	Short-span	Corner	Long-span	Short-span
A10R15L3-1	0.67	0.87		0.49	0.60	
A10R15L3-2	0.85	0.99				
A10R30L3-1	0.78	0.78		0.43	0.55	
A10R30L3-2	0.56	0.92				
A10R15L5-1	0.24	0.89		0.24	0.57	
A10R15L5-2	0.50	0.89				
A10R30L5-1	0.60	0.99		0.41	0.56	
A10R30L5-2	0.66	0.74				
A15R15L3-1	0.49	0.83	0.99	0.29	0.50	0.57
A15R15L3-2	0.41	0.71	0.77			
A15R30L3-1	0.57	0.75	0.96	0.33	0.38	0.53
A15R30L3-2	0.45	0.44	0.68			
A15R15L5-1	0.26	0.60	0.81	0.34	0.46	0.61
A15R15L5-2	0.78	0.83	1.09			
A15R30L5-1	0.44	0.70	0.88	0.38	0.48	0.61
A15R30L5-2	0.73	0.77	1.01			
A20R15L3-1	0.23	0.63	0.98	0.25	0.40	0.67
A20R15L3-2	0.55	0.61	1.09			
A20R30L3-1	0.73	0.55	1.03	0.49	0.39	0.64
A20R30L3-2	0.80	0.65	0.94			
A20R15L5-1	0.42*	0.60	1.03	0.28	0.37	0.58
A20R15L5-2	0.46	0.54	0.77			
A20R30L5-1	0.45	0.79	1.33	0.34	0.43	0.73
A20R30L5-2	0.60	0.55	0.94			

*One of the corners strain gauges were excluded from the calculation of the average hoop rupture strain.

Table 5. Variation of strain reduction factor with sectional aspect ratio and corner radius

h/b	R=15			R=30			$(R)_{all}^{*}$		
	$k_{\varepsilon\text{-short}}$	$k_{\varepsilon\text{-long}}$	$k_{\varepsilon\text{-corner}}$	$k_{\varepsilon\text{-short}}$	$k_{\varepsilon\text{-long}}$	$k_{\varepsilon\text{-corner}}$	$k_{\varepsilon\text{-short}}$	$k_{\varepsilon\text{-long}}$	$k_{\varepsilon\text{-corner}}$
1.0	0.59		0.36	0.55		0.42	0.57		0.39
1.5	0.59	0.48	0.31	0.57	0.43	0.35	0.58	0.45	0.33
2.0	0.62	0.38	0.27	0.68	0.41	0.42	0.65	0.40	0.34
$(h/b)_{all}^{*}$	0.60	0.48	0.31	0.60	0.47	0.40	0.60	0.47	0.36

*$(h/b)_{all}$ = average values for specimens with different aspect ratios; $(R)_{all}$ = average values for specimens with different corner radii

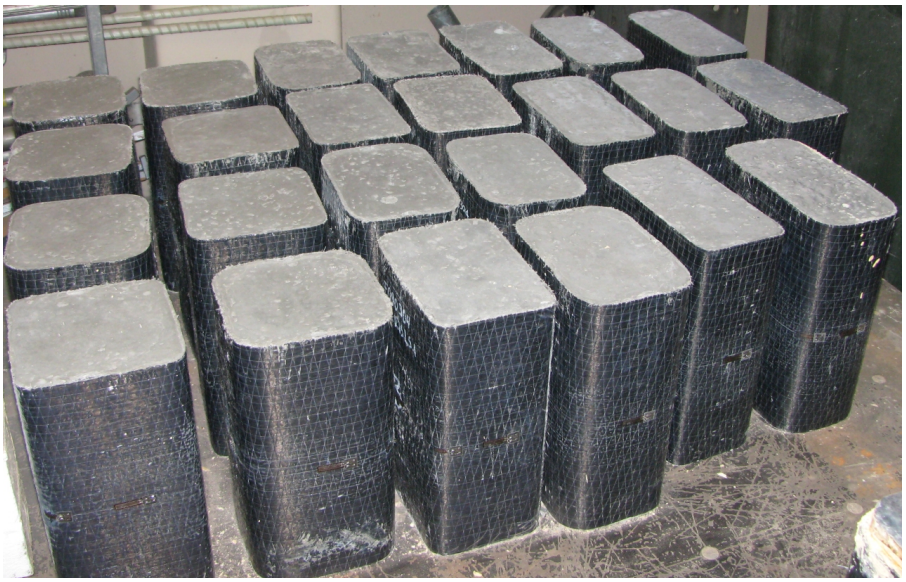

Figure 1. Specimens before testing

Figure 2. Test setup and instrumentation

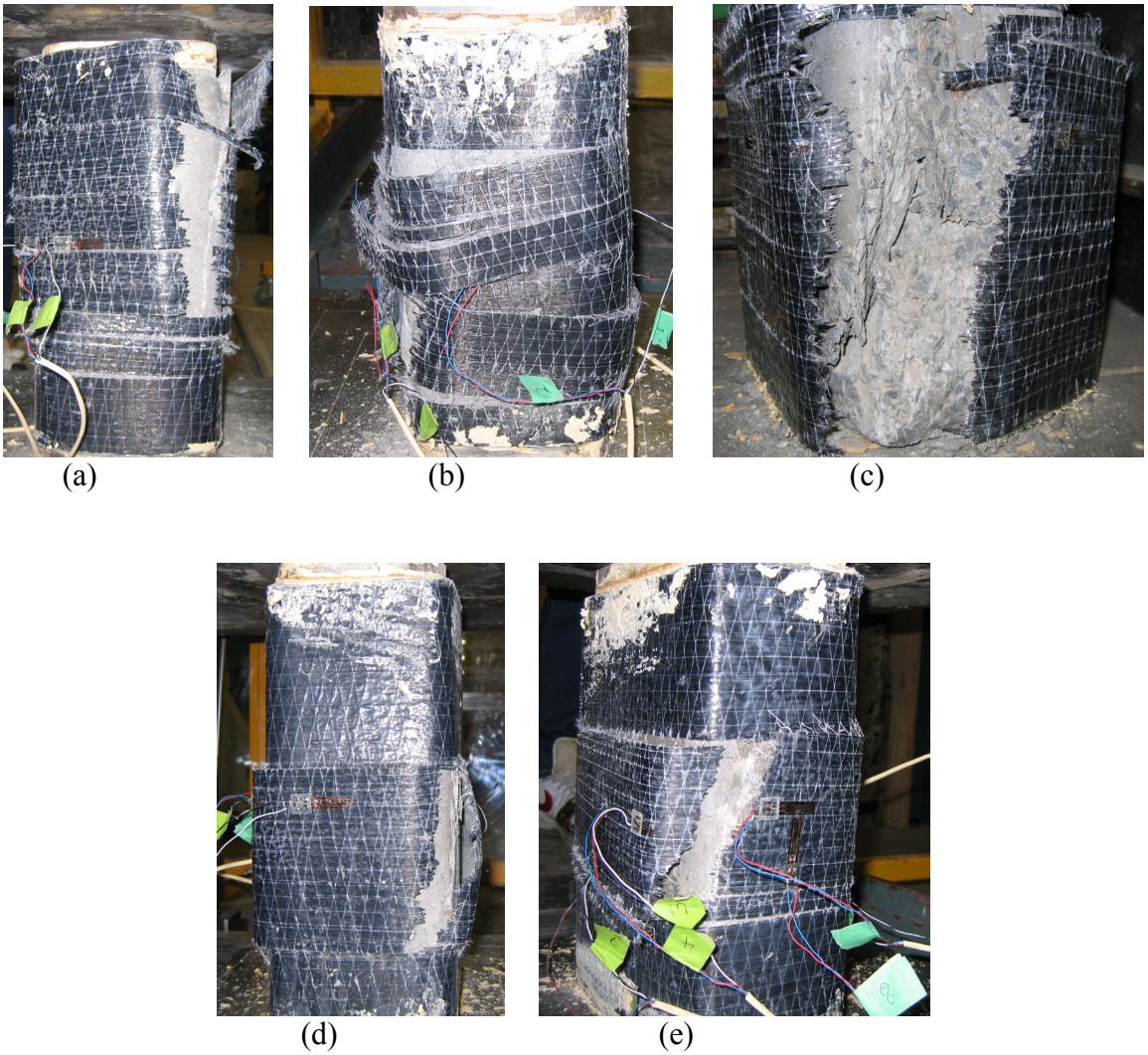

Figure 3. Failure modes of specimens: a) A10R30L3-2; b) A10R30L5-1; c) A15R15L3-2; d) A15R15L5-2; e) A20R15L3-2

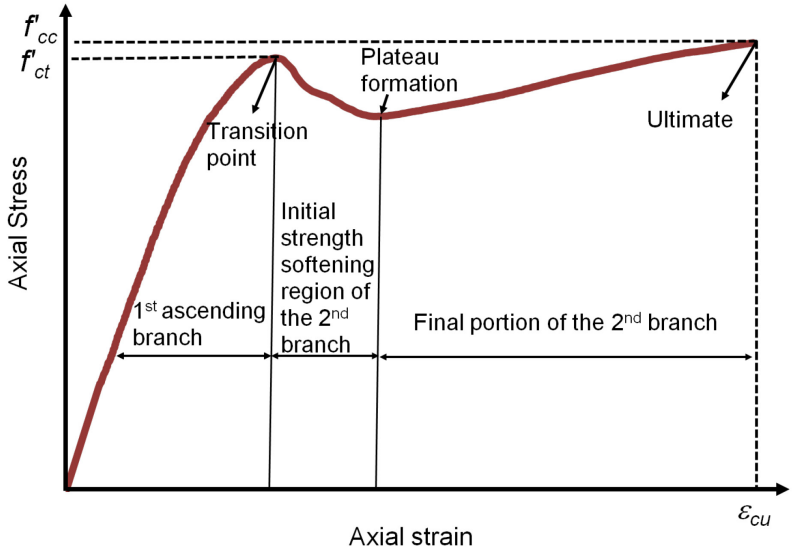

Figure 4. Illustration of different stages of axial stress-strain curves

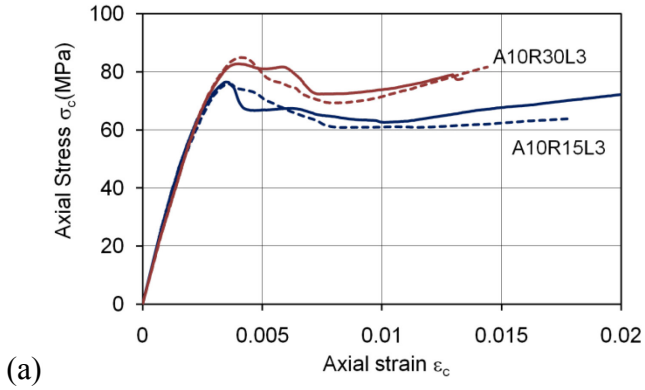

(a)

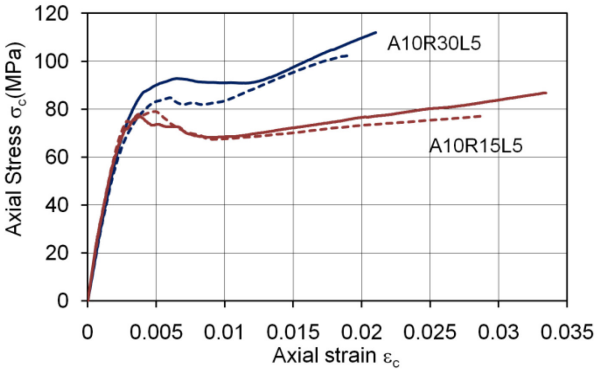

(b)

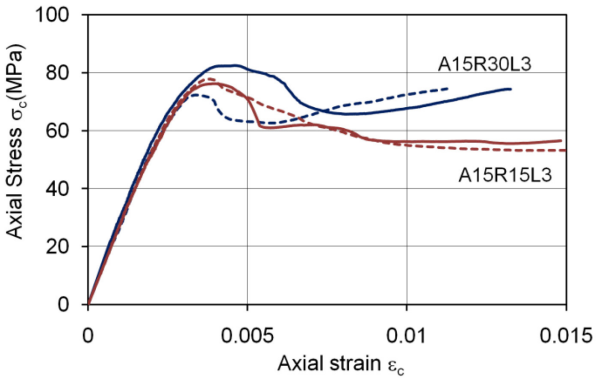

(c)

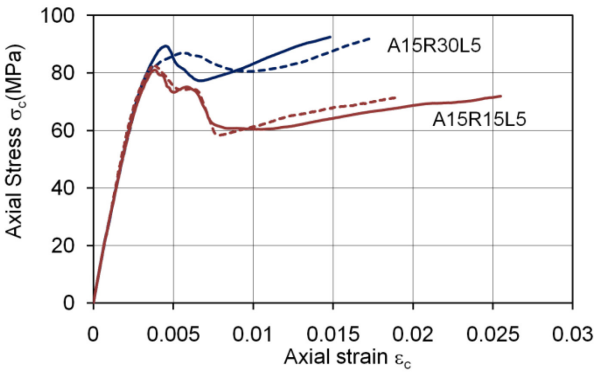

(d)

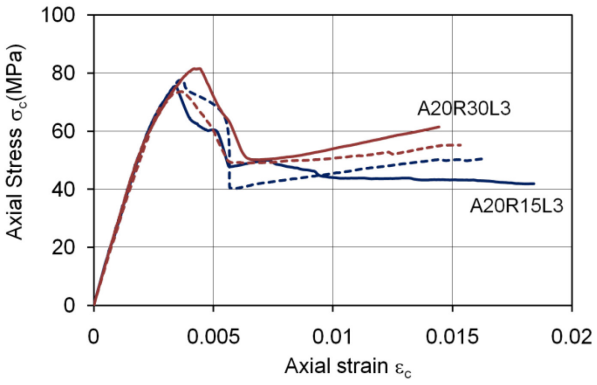

(e)

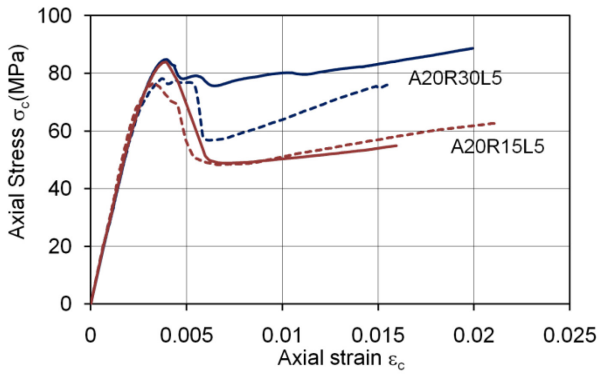

(f)

Figure 5. Influence of corner radius on axial stress-strain curves: a) h/b=1.0, L=3; b) h/b=1.0; L=5; c) h/b=1.5, L=3; d) h/b=1.5, L=5; e) h/b=2.0, L=3; f) h/b=2.0; L=5

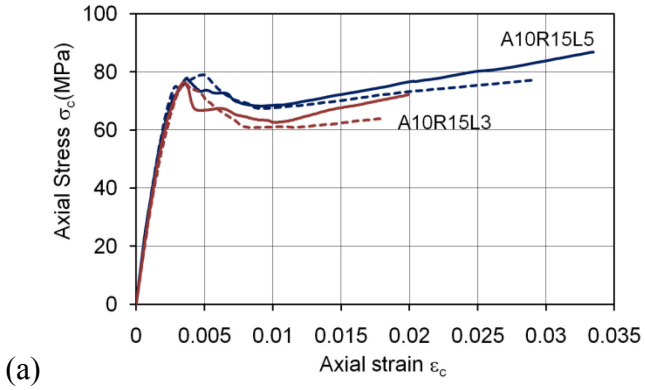

(a)

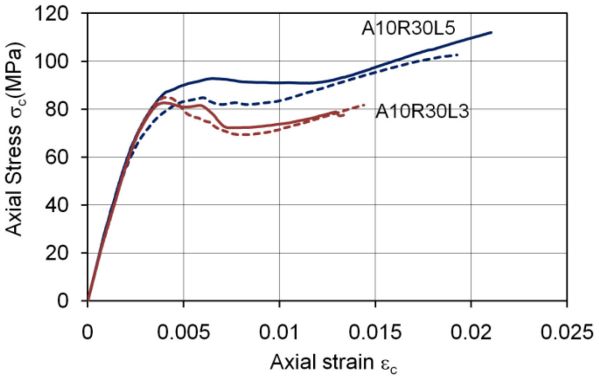

(b)

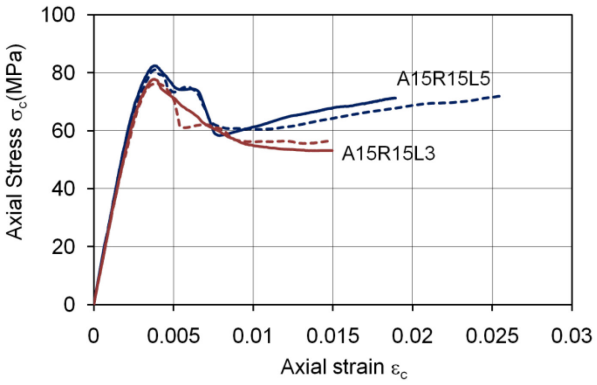

(c)

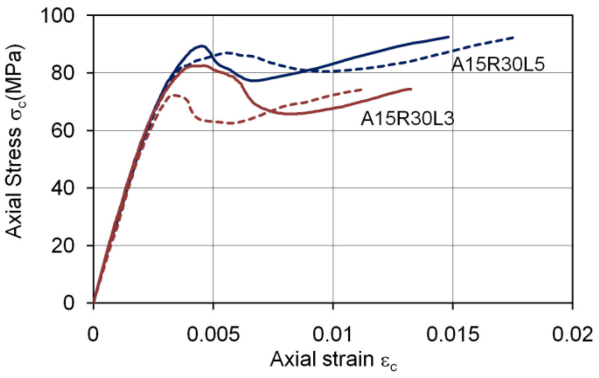

(d)

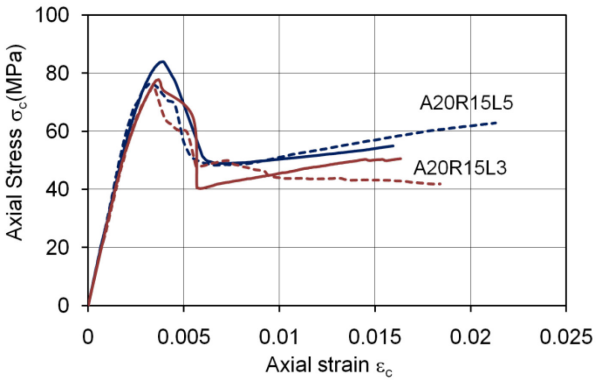

(e)

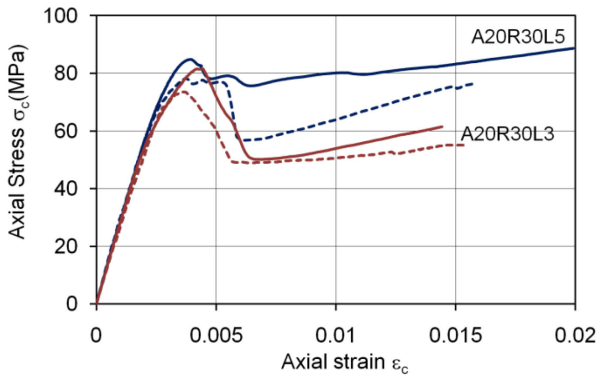

(f)

Figure 6. Influence of number of FRP layers on axial stress-strain curves: a) h/b=1.0, R=15 mm; b) h/b=1.0, R=30 mm; c) h/b=1.5, R=15 mm; d) h/b=1.5, R=30 mm; e) h/b=2.0, R=15 mm; f) h/b=2.0, R=30 mm

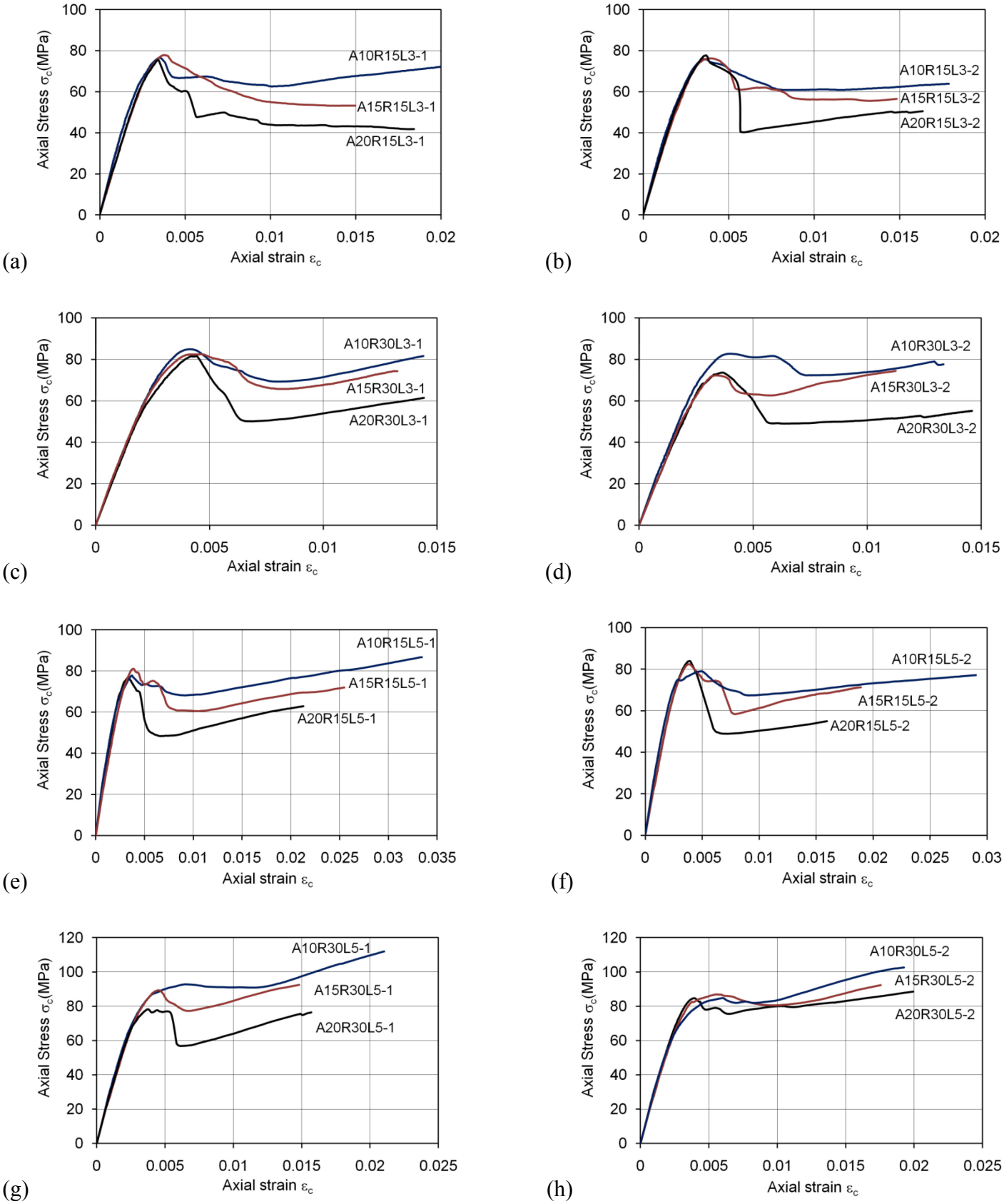

Figure 7. Influence of sectional aspect ratio on axial stress-strain curves: a) R=15 mm, L=3, series 1; b) R=15 mm, L=3, series 2; c) R=30 mm, L=3, series 1; d) R=30 mm, L=3, series 2; e) R=15 mm, L=5, series 1; f) R=15 mm, L=5, series 2; g) R=30 mm, L=5, series 1; h) R=30 mm, L=5, series 2